Lietzén, J.; Liljemark, A.; Duan, R.; Jäntti, R.; Viikari, V.

Polarization Conversion -based Ambient Backscatter System

Published in:
IEEE Access

DOI:
10.1109/ACCESS.2020.3042018

Published: 01/01/2020

Document Version
Publisher's PDF, also known as Version of record

IEEE Access
Multidisciplinary ⋮ Rapid Review ⋮ Open Access Journal

Received November 13, 2020, accepted November 24, 2020, date of publication December 2, 2020, date of current version December 14, 2020.

Digital Object Identifier 10.1109/ACCESS.2020.3042018

Polarization Conversion-Based Ambient Backscatter System

JARI LIETZÉN[1], ALEKSI LILJEMARK[1], RUIFENG DUAN[1], (Member, IEEE), RIKU JÄNTTI[1], (Senior Member, IEEE), AND VILLE VIIKARI[2], (Senior Member, IEEE)

[1]Department of Communications and Networking, Aalto University, 02150 Espoo, Finland
[2]Department of Electronics and Nanoengineering, Aalto University, 02150 Espoo, Finland

Corresponding author: Jari Lietzén (jari.lietzen@aalto.fi)

This work was supported in part by the Academy of Finland under Grant 311760.

ABSTRACT In Ambient Backscatter Communications (AmBC), a backscatter device communicates by modulating the ambient radio frequency (RF) signal impinging at its antenna. In many cases, the system setup is bi-static such that the receiver and the ambient signal source are separated in space. This configuration suffers from the direct path interference problem. The direct signal component can be several orders of magnitude stronger than the scattered one. This imposes a challenge for the receiver that needs to have high dynamic range in order not to lose the scattered signal component to the quantization noise. In this paper, we propose a novel AmBC system concept, in which a polarization conversion between the direct and scattered path is introduced at the backscatter device and exploited at the dual polarization based receiver antenna to mitigate the direct path interference. The proposed system is agnostic to the ambient signal source characteristics as long as it uses linearly polarized antennas. The backscatter device changes the polarization from linear to circular. The receiver antenna is a circularly polarized patch antenna with a 180°-hybrid to obtain the difference between the left- and right-hand polarized fields. Ideally, this receiver antenna and 180°-hybrid combination would completely remove linearly polarized direct path and reflected components. In this paper, we propose a robust design that can mitigate the direct path signal power more than 25 dB despite nonidealities in the antenna manufacturing.

INDEX TERMS Polarization conversion, ambient backscatter communication.

I. INTRODUCTION

Backscattering radio waves from an object has been a subject of active study since the development of radar technologies back in the 1930's, and the use of backscattered radio for communications since Harry Stockman's work in 1948 [1]. Backscatter Communication (BC) technology has been widely used in radio frequency identification (RFID) communication systems, where a reader device generates an unmodulated carrier signal, a passive tag absorbs the energy of this signal and then sends back the modulated signal to the reader. Utilizing the existing ambient radio frequency in the air, ambient backscatter communication (AmBC), a new communication technology, has been developed by researchers at University of Washington in 2013 [2]. Several ambient signals can be used as the carrier in AmBC including frequency modulation (FM) [3], [4] and TV broadcasts [2], [5], [6] as well as Bluetooth [7]–[9] and WiFi transmissions [10]–[13].

The BC and AmBC system deployments can be either monostatic, where transmit and receive antennas are co-located, or bi-static, where transmit and receive antennas are separated in space. In the latter case, the backscatter-modulated signal is superimposed with the direct path signal component at the receiver. In many practical AmBC deployments, the received power from the direct signal path is several orders of magnitude larger than that of the desired signal component of the AmBC system [14]. This imposes a challenge to the backscatter receiver design that needs to have a large dynamic range in order not to lose the backscatter message into the quantization noise of the analog-to-digital converter (ADC) or distortion products due to receiver

The associate editor coordinating the review of this manuscript and approving it for publication was Shah Nawaz Burokur.

amplifier saturation [15], [16]. A contemporary survey of AmBC systems is presented in [17] discussing issues and limitations of AmBC systems.

The strong direct path signal appears as an interference to the AmBC demodulator. Several techniques have been proposed to mitigate the impact of the direct path interference, such as using long symbol duration to improve the signal-to-noise-plus-interference ratio (SINR) of the scattered signal at the receiver, shifting the backscattered signal to a different frequency band [18], [19] and using multiple receiver antennas [20]–[22]. More recently, hybrid beamforming techniques, machine-learning assisted detection approaches together with coding schemes have been applied to AmBC systems to promote the applications of AmBC in practice [15], [16].

One technique for minimizing the effect of the strong ambient RF signal is to shift the radio frequency on which the backscatter communication system operates away from the one of the ambient RF signal. This approach has been utilized to co-exist with WiFi in [11], [23] and with LoRA [24]. In [25], [26] a multi-hop protocol was proposed, in which each of the backscatter devices in the multi-hop-chain between the transmitter and receiver shift the frequency further. In [18], [19], partial shift of the spectrum was proposed for Orthogonal Frequency Division Multiplexed (OFDM) ambient signals, such that the scattered component would appear in the null carriers of the ambient signal. The drawback of these frequency shifting approaches is that they assume that there is interference free spectrum white space available where the scattered component can be shifted. Frequency shifting at the backscatter device also has a power consumption cost that can be significant in case the device is powered through RF energy harvesting.

Another mean of avoiding the strong interference caused by the ambient RF signal is to adopt interference cancellation techniques. In [27], a simple two antenna receiver was proposed that utilized analog components and avoided the use of analog-to-digital converter. The drawback of the design is that it is suitable only for envelope detector type of receiver. In [15], a more complicated multi-antenna receiver structure was proposed in which the direct path signal component is first nulled in the analog domain and then digital beamformer receiver is utilized for the AmBC signal. Moreover, authors in [16] proposed a machine learning-assisted method using classification algorithms for extracting the information of the AmBC device, while the considered legacy system was operating with normal signal-to-noise (SNR) regime. The design enables the AmBC system to retrieve the binary phase shift keying (BPSK) modulated information with practically acceptable performance without having the knowledge of the channel information and the constellations of the unknown Gaussian-distributed ambient RF signals of the legacy system.

The authors in [28] propose a polarization-based reconfigurable (PR) antenna design to improve the backscatter modulated signal path over the direct signal path. The PR antennas are able to switch between several linear polarizations. When the backscatter modulator sends a message several times using different polarizations, the possibility of receiving at least one good quality copy of the message is increased. By selecting the antenna polarization at the receiver end to be orthogonal to the ambient transmitter's antenna polarization, it is in theory possible to completely remove the direct signal coming from the ambient transmitter.

The receiver antenna design most related to ours has been proposed in [29] applying antenna polarization technique. The authors have designed a passive backscatter communication system with wide-band antenna circuits for receiving the ambient and backscattered signals. The backscatter signal is polarized and then delayed. The two received signals are coupled to a mixer to extract the modulated signal. However, the backscatter device is equipped with one antenna to receive the ambient signal and another antenna for transmitting the modulated signal. The system offers a simple way to mitigate the direct path signal at the receiver, but suffers from the need of two antennas at the transponder and is only applicable with ambient signals whose polarization matches to that of the transponder receiving antenna.

In this paper, we propose a novel AmBC system concept, in which a polarization conversion between the direct and scattered path is introduced at the backscatter device and is exploited at the dual-polarized receiver to cancel the direct path and reflected components. The proposed system is agnostic to the ambient signal source characteristics as long as it uses linearly polarized antennas. The backscatter device changes the polarization from linear to circular. The receiver antenna is a circularly polarized patch antenna with a 180°-hybrid to obtain the difference between the left- and right-hand polarized fields. Ideally, the transponder would fully convert the ambient energy at a linear polarization to the circularly-polarized modulated signal. Our contribution is to apply polarization conversion techniques to improve the AmBC system performance. Particularly, the ambient signals are unknown and usually very strong compared to the backscattered signals. Hence, the useful signal is embedded into strong interference and therefore it is challenging to design a receiver to retrieve the useful signal without utilizing complex and advanced techniques [14]. The operating principle of our concept can be implemented using different building blocks, as the operation does not depend on any specific design detail of those building blocks. These building blocks include commercial antennas and hybrid components, or readymade polarization converters. A polarization converter converting linear polarization to circular one can be used as the backscatter device if it is possible to control the conversion, i.e. to switch the conversion ON and OFF. The antennas with suitable hybrid circuits for the backscatter device and the receiver could be made cost efficiently on ordinary circuit boards, as we will later demonstrate.

In this paper, we propose a transponder design that provides 25 dB improvement in the modulated signal to direct path interference ratio in an anechoic environment. Signals reflected from the environment are also received by the dual-polarized receiver and are being cancelled like the direct path component. In a practical environment, reflections can alter the signal polarization and therefore the environment largely defines how much the signal to direct path interference -ratio can be improved.

The rest of the paper is organized as follows. In Section II, we introduce the operation principle of our proposed AmBC system. Section III outlines the design principles of the polarization conversion based receiver and the proposed antenna configuration. In Section III-B, we briefly present the operation principle of the backscatter device. We conduct the frequency sensitivity analysis of the polarization conversion based receiver in Section IV. The evaluation of the design with respective to measurements in an an-echoic RF-chamber are provided in Section V. Section VI concludes this paper with discussion on achieved results and limitations of the current design.

II. SYSTEM CONCEPT

Consider an AmBC system consisting of an ambient signal source, such as a broadcast transmitter, a backscatter device and a receiver. The backscatter device modulates the ambient signal impinging at its antenna, performing e.g. on-off keying (OOK) as in [2]. The receiver sees super-position of the direct signal component coming from the ambient source and the backscatter device modulated signal component. In a bi-static case, the transmitter and the receiver are not co-located, so strictly speaking the term backscatter is not a correct one as the signal is not necessarily scattered to the direction where the signal came from. We will slightly abuse the term and denote scattering from the antenna of the modulating device to the direction of the receiver. In the monostatic case, the direct signal component is typically weak due to full-duplex antenna design, but in the bi-static case it can be several orders of magnitude stronger than the scattered signal.

A circularly polarized antenna is an attractive choice for the receiver antenna as it is very effective removing multi-path interferences [30]. Another advantage is that no strict orientation between transmitting and receiving antennas is required, which is a problem with linearly polarized antennas [30]. A case study presented in [30, p. 271] shows a Printed Quadrifilar Helix Antenna (PQHA) capable of maintaining good circular polarization at 2 GHz over the vertical theta (θ) angle of about 140°.

In free-space, the direct path power transfer between the transmitter and receiver antennas can be expressed using Frii's equation as:

$$p_d = G_r \left(\frac{\lambda}{4\pi R} \right)^2 G_t p_t, \tag{1}$$

where λ denotes the wavelength, R is the distance between the transmitter and the receiver antennas, G_r is the receiver antenna gain, G_t is the transmitter antenna gain, and p_t is the transmitted power. In case of including a backscatter device, the power transfer of the compound link, i.e. transmitter-backscatter-receiver, can be written as [31]

$$p_b = G_r \left(\frac{\lambda}{4\pi R_2} \right)^2 M \left(\frac{\lambda}{4\pi R_1} \right)^2 G_t p_t, \tag{2}$$

where R_1 is the distance from transmitter to the backscatter device, R_2 is the communication distance from the backscatter device to the receiver, and M is the modulation factor (modulation and antenna losses) of the backscatter device.

The received signal power is

$$p_r = p_b + p_d + p_z, \tag{3}$$

where the term p_z denotes the instantaneous additive white Gaussian noise power at the receiver. If the ambient source signal has time varying amplitude, then p_d is time-varying and therefore difficult to cancel. We also note that

$$\frac{p_b}{p_d} = M \left(\frac{\lambda}{4\pi} \frac{R}{R_1 R_2} \right)^2 \ll 1 \tag{4}$$

for practical values of the distances, which means that the receiver should have high dynamic range in order not to lose the desired backscattered signal component due to receiver saturation or quantization noise.

So far we have not considered the effect of polarization mismatches between the antennas. The polarization mismatch between two elliptical polarization waves is given by [32]:

$$X = \frac{1}{2} \left(1 + \frac{4r_1 r_2 + (1 - r_1^2)(1 - r_2^2)\cos(2\beta)}{(1 + r_1^2)(1 + r_2^2)} \right), \tag{5}$$

where r_k, $1 \leq |r_k| < \infty$, denote the ellipticity ratio, i.e., the signed voltage ratio of the major axis of the polarization ellipse to its minor axis for the transmitter ($k = 1$) and the receiver ($k = 2$) antennas. The parameter β is the polarization mismatch angle $0 \leq \beta \leq \pi/2$. For linearly polarized antenna $|r_k| \to \infty$, and for a circularly polarized antenna $|r_k| \to 1$. In practice, linearly polarized antennas have $|r_k| < \infty$, and circularly polarized antennas have $|r_k| > 1$.

Assume that the ambient source applies linear polarization. The backscatter device has a linearly polarized input antenna connected to a circularly polarized output antenna through a circulator and an RF switch. We will present the design of such a device in Section III-B. We consider that the receiver is able to receive the left-hand and right-hand circularly polarized components separately. The receiver uses the Stokes parameter $V \triangleq \langle E_{CL}^2 \rangle - \langle E_{CR}^2 \rangle$ measuring the field strength difference between left- and right-hand circularly polarized fields (denoted as CL and CR, respectively) for detecting the backscatter signal. In Section III, we will discuss how such a receiver antenna structure can be designed.

If the backscatter device is in 'off' state ($p_b \approx 0$), the circularly polarized components are weak and $V \approx 0$. When the backscatter device is in 'on' state, there is one strong circularly polarized component. Say that the backscatter antenna is left-hand circularly polarized. Then in 'on' state, we have $V > 0$. Hence, V can be used as the measurement to detect the state of the backscatter antenna and thus demodulate OOK symbols. In case of an ideal dual polarization receiver, the measurement V will be independent on the linearly polarized direct signal components that are not modulated by the backscatter device. Assuming an ideal anechoic free-space propagation environment, the received signal power at the output of the dual polarization receiver is given by

$$p_r = (X_{L\to CL} - X_{L\to CR})p_d + (X_{CL\to CL} - X_{CL\to CR})X_{L\to b}p_b + p_z, \quad (6)$$

where $X_{CL\to CL}$ is the polarization match from the left-hand circularly polarized backscatter antenna to the left-hand circularly polarized arm, and $X_{L\to CL}$ and $X_{L\to RL}$ denote the polarization losses from the linearly polarized transmit antenna to the left- and right-hand circularly polarized receiver antennas, respectively. The parameter $X_{L\to b}$ is the polarization mismatch between the backscatter antenna and the linearly polarized transmit antenna. Ideally, since $X_{L\to CR} \approx X_{L\to CL}$, $X_{CL\to CR} \approx 0$, and $X_{CL\to CL} \approx 1$, we have $p_r \approx X_{L\to b}p_b + p_z$. This is the direct signal path that will be completely removed by the dual polarization receiver.

The polarization loss between the linearly polarized wave ($|r_1| = \infty$) and the elliptical polarized antenna ($|r_2| = |r| \approx 1$) is given by

$$X_{L\to E} = \frac{1}{2}\left(1 + \frac{1-r^2}{1-r^2}\cos(2\beta)\right). \quad (7)$$

Ideally, both arms of the dual polarization receiver have the same ellipticity such that $X_{L\to CL} = X_{L\to CR} = X_{L\to E}$. The sensitivity of the polarization loss to the antenna parameter r becomes

$$\frac{d}{dr}X_{L\to E} = -\frac{r}{(1+r^2)^2}\cos(2\beta). \quad (8)$$

Hence, a small deviation in r, δ_r, between the two arms of the dual polarization receiver results in

$$(X_{L\to CL} - X_{L\to CR}) \approx \frac{1}{4}\delta_r, \quad (9)$$

while assuming $\beta = 0$. With $\delta_r = 0.1$, we obtain approximately 16 dB reduction to the direct path power. With $\delta_r = 0.01$, the obtained reduction is approximately 26 dB. Hence, the expected damping of the direct path signal is significant, which dramatically reduces the required dynamic range of the receiver.

III. POLARIZATION CONVERSION -BASED BACKSCATTER RECEIVER

A. ANTENNA SYSTEM

If the receiver uses two separate antennas, one for receiving a left-hand circularly polarized signal and the other for receiving a right-hand circularly polarized signal, a 180°-hybrid can be adopted to subtract the signals from each other. This arrangement expects the two antennas to be identical and co-located. The schematic drawing for a 180°-hybrid is shown in Fig. 1. It is a four-port network and the input signal at

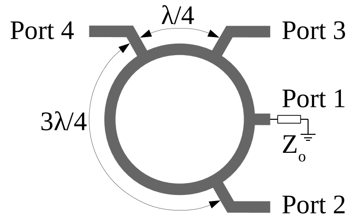

FIGURE 1. Schematic drawing of a 180°-hybrid.

port 4 is equally split in amplitude between ports 2 and 3 but there is a 180° phase difference [33]. Ideally, no power is directed to port 1, but in case of mismatches in other ports the port 1 should be terminated to its characteristic impedance. We consider connecting the antenna receiving a left-hand circularly polarized signal to port 2 and the antenna receiving right-hand circularly polarized signal to port 3, and using the port 4 as an output. Hence, the scattering matrix for the ideal hybrid reads [33]

$$\mathbf{S} = \frac{-j}{\sqrt{2}}\begin{bmatrix} 0 & 1 & 1 & 0 \\ 1 & 0 & 0 & -1 \\ 1 & 0 & 0 & 1 \\ 0 & -1 & 1 & 0 \end{bmatrix}. \quad (10)$$

Assuming the incoming signal is either left-hand or right-hand circularly polarized and multiplying the input signals with the scattering matrix shows that the incoming signals are divided between the output port 4 and the terminated port 1. If the ambient transmitter is not using circular polarization, and we assume the two receiving antennas to be identical, the input signal is equal for both antennas. Multiplying the input signal with the scattering matrix shows that all the ambient transmitter's signal is directed to port 1 and is absorbed in the terminating resistor. No signal is seen at the port 4.

The 180°-hybrid works well in removing the ambient transmitter's signal, but the receiving antennas need to be identical. To overcome the challenges in manufacturability, an antenna design that incorporates both antennas in one physical element is preferable. One such candidate is shown in Fig. 2. A single microstrip antenna with two feeding points combined with a quadrature hybrid is capable of receiving circularly polarized signals [34]. The schematic drawing of a quadrature hybrid is shown in Fig. 3. The input signal fed into port 2 or 3 is equally split in amplitude between ports 1 and 4 with, however, a 90° phase difference. The scattering matrix for such a quadrature hybrid is [33]

$$\mathbf{Q} = \frac{-1}{\sqrt{2}}\begin{bmatrix} 0 & j & 1 & 0 \\ j & 0 & 0 & 1 \\ 1 & 0 & 0 & j \\ 0 & 1 & j & 0 \end{bmatrix}. \quad (11)$$

When the antenna in Fig. 2 is used at the receiver, the left-hand circularly polarized signal appears at port 2 and the right-hand circularly polarized signal at port 3. The ports 2 and 3 from the quadrature hybrid are connected to the

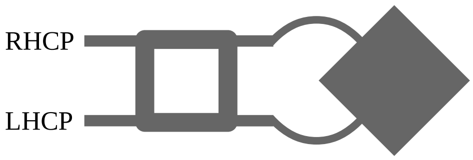

FIGURE 2. A dual-feed circularly polarized rectangular microstrip antenna.

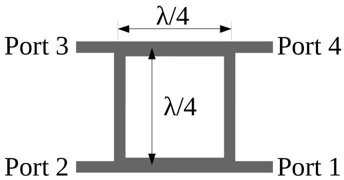

FIGURE 3. Schematic drawing of a quadrature hybrid.

corresponding ports in the 180°-hybrid. The signals from the antenna are now connected to ports 1 and 4 of the quadrature hybrid. The ambient transmitter's signal **a** is still completely removed, there is no signal at port 4 of the 180°-hybrid. Therefore,

$$\mathbf{a} = \begin{bmatrix} 1 & 0 & 0 & 1 \end{bmatrix}, \tag{12}$$

$$\mathbf{P_r} = \mathbf{S}(\mathbf{Q}\mathbf{a}^{\mathsf{T}}) = \begin{bmatrix} -1+j & 0 & 0 & 0 \end{bmatrix}^{\mathsf{T}}. \tag{13}$$

Figure 4 summarizes power transfer in an ideal case between antennas that are using different linear or circular polarizations. The operating principle of our proposed receiver antenna and the 180° hybrid construction is illustrated on the lower right part of Fig. 4. Only the circularly polarized input signal produces an output signal whereas all linearly polarized signals are canceled at the receiver. This cancellation works perfectly regardless whether the linearly polarized signals are coming directly from the ambient transmitter or are reflections with unknown polarization angles.

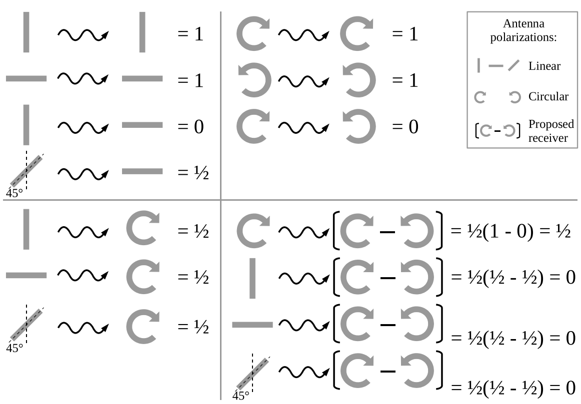

FIGURE 4. Power transfer between antennas using different polarizations.

A prototype antenna and 180° hybrid construction for 2.44 GHz center frequency is shown in Fig. 5.

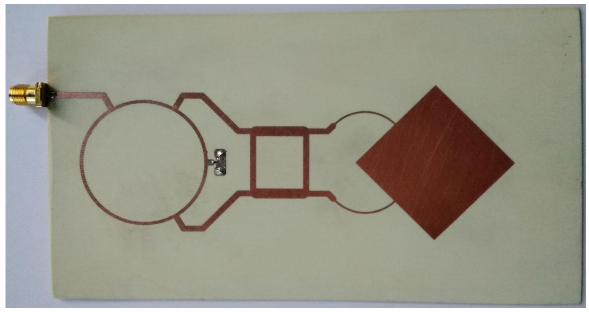

FIGURE 5. A prototype antenna for 2.44 GHz to be used at the receiver.

B. BACKSCATTER DEVICE DESIGN

In the proposed design, the backscatter device has a linearly polarized input antenna connected to a circularly polarized output antenna through a modulator. The operation principle of the backscatter device is illustrated in Fig. 6. The modulator is a voltage controlled RF-switch and the controller is realized using a microcontroller to generate the modulating waveform. The RF-switch used in this design is a non-reflective single pole double throw (SPDT) or a change-over switch. The functional diagram of the RF-switch is shown in Fig. 7. As the modulation is realized by either connecting the two antennas together or isolating them from each other, the non-reflective construction of the RF-switch helps to minimize unwanted backscattering when the antennas are not connected together. The receiving antenna is connected to port marked as RFC on the RF-switch and the transmitting

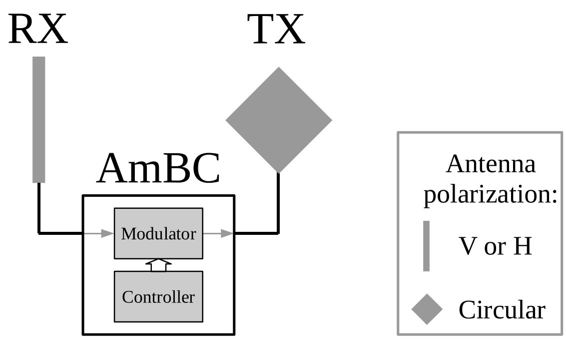

FIGURE 6. Block diagram of the backscatter device.

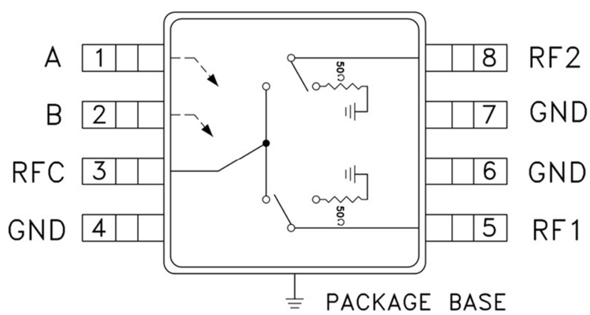

FIGURE 7. Functional diagram of the RF-switch [35].

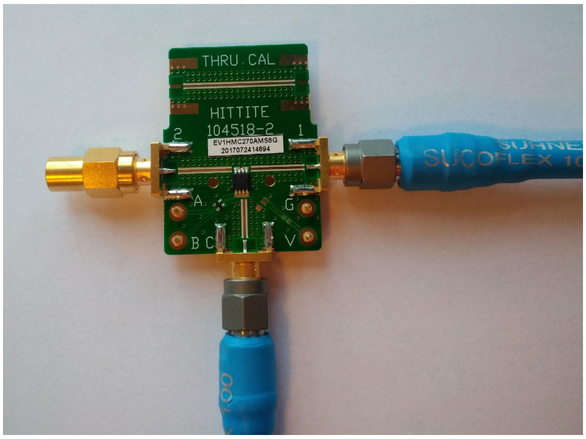

FIGURE 8. The evaluation board for the RF-switch.

antenna is connected to port RF1. When the antennas are not connected together, port RF1 is terminated with its characteristic impedance. The port RFC is now connected to port RF2 and it has to be terminated with its characteristic impedance. Without the terminations, there is a possibility that the antennas are reflecting the incoming signal back. This would degrade the performance of the backscatter device by introducing a background backscattering signal. It is possible that the modulated signal leaks from the circularly polarized output antenna back to the linearly polarized input antenna, forming a loop back. However, there is a 3 dB attenuation due to the polarization mismatch between linear and circular polarization and the insertion loss of the RF-switch is added to the total attenuation of the loop causing the loop back signal to fade rapidly. The insertion loss of the RF-switch at 2.44 GHz is 1.0 dB [35]. Antennas also have a structural mode in addition to the antenna mode [36]. The structural mode does not cause currents at the antenna feed and thus are rescattering the direct signals. This rescattering is not part of the modulated signal, but rather appears as a constant background backscattered signal at the receiver.

A commercially available evaluation board for the selected RF-switch was used to conduct the measurements [35]. The evaluation board is seen in Fig. 8. The 50 Ω termination resistor is seen on the left side of the circuit board. The switch is controlled with control ports A and B visible in figures 7 and 8. To feed the signal from the receiving antenna on port RFC to the transmitting antenna on port RF1, port A is connected to voltage of −5 V relative to ground, and port B to 0 V. To feed the signal from RFC to the terminated port RF2, port A is connected to 0 V and port B to −5 V.

C. COMPARISON OF DIFFERENT RECEIVER CONCEPTS

In bi-static AmBC systems the strong direct path signal appears as an interference to the AmBC receiver. In addition, reflected signals originating from the ambient transmitter are also interfering with the same receiver. It is therefore desirable that the receiver can at least attenuate the interfering signals and in an ideal case be able to remove them

TABLE 1. Comparison of different receiver concepts.

Concept	Path 1	Path 2	Path 3	Ref.
	$\frac{1}{2}$	$\frac{1}{2}$	$\frac{1}{2}$	
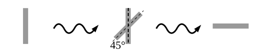	$\frac{1}{2}\cdot\frac{1}{2}=\frac{1}{4}$	0	$f(\phi)$	[28]
	$\frac{1}{2}$	0	0	

Signal paths
1: Ambient transmitter → Backscatter device → Receiver
2: Ambient transmitter → Receiver
3: Ambient transmitter → Reflection → Receiver

completely. In Table 1, three receiver concepts with different antenna polarizations are compared to each other according to their power transfer efficiency, as well as resistance to both the direct path and reflected path signal components.

The polarization mismatch problem becomes a factor when the antenna polarizations of the ambient transmitter, the backscatter modulator and the receiver differ from each other [17, p. 2894]. While polarization mismatch between the ambient transmitter and the receiver can be used to remove the interfering direct path signal as in [28], a mismatch between the backscatter modulator and the receiver decreases the received power.

The first concept presented in Table 1 uses circular polarization at the receiver while the backscatter modulator and the ambient transmitter are using linear polarizations. While the orientation of the backscatter modulator is no longer an issue, the received power is now halved. Also, there is no improvement regarding the direct path signal or reflected signal components other than the same halving of input power.

The concept proposed in [28] offers in theory a perfect cancellation of the direct path signal. An example based on the proposed PR antenna design is listed as the second concept in Table 1. Here, the polarization selection of the ambient transmitter and the receiver results in a perfect cancellation of the direct path signal. However, the polarization selection also results in an unavoidable power loss to the useful signal due to polarization mismatch between the ambient transmitter and the backscatter modulator and a second time between the backscatter modulator and the receiver. As claimed in [28], the use of a PR antenna also significantly reduces the effect of reflected signals as the receiver is able to select among several messages transmitted using different antenna polarizations. Unfortunately, the angle of the reflections cannot be controlled, thus the reduction of the reflected signals will always be a function of the polarization angle ϕ of the reflection.

The third concept in Table 1 is our proposed AmBC system. The signal path from the ambient transmitter to the backscatter modulator and finally to the receiver does not suffer from additional power loss as there are no polarization mismatches between the steps. There is a 3 dB power reduction due to the 180°-hybrid. As with the second concept, our proposed system is also able to completely remove the direct path signal. The reflected signals, although their polarization angles vary, are in theory completely removed as well as shown in (13).

IV. FREQUENCY SENSITIVITY ANALYSIS

The functional analysis in the previous section was based on the assumption that all the components are ideal. However, the construction of a 180°-hybrid and a quadrature hybrid on a circuit board is frequency dependent. If the operating frequency deviates from the design frequency, the removal of the ambient signal is no longer perfect. The scattering matrices for the ideal hybrids can be found on numerous textbooks, Equations (10) and (11) respectively, but now we need to analyze the non-ideal situation where the hybrids' operating frequency deviates from the design frequency in order to find out the usable bandwidth where the removal of the ambient signal is still large enough.

The properties of a quadrature hybrid can be analyzed using an even- and odd-mode analysis. The quadrature hybrid has a symmetry plane as shown in Fig. 9. The quadrature hybrid is divided in two two-port networks along the symmetry plane and it suffices to analyze only one of the two-port networks. The two-port network for even- and odd-mode analysis is shown in Fig. 10. The two-port network is split up into its three parts: a $\lambda/8$ stub, a $\lambda/4$ transmission line, and a second $\lambda/8$ stub. The stubs and transmission line segments are set to correspond to the wavelength at the design frequency. For an even-mode analysis, the stubs are left open and for odd-mode analysis the stubs are short circuited. The quadrature hybrid is analyzed in terms of two equivalent two-port networks, one for even-mode and one for odd-mode. The complete solution is obtained by combining the even- and odd-mode scattering parameters. The hybrid circuits are analyzed in detail in [33] and [37].

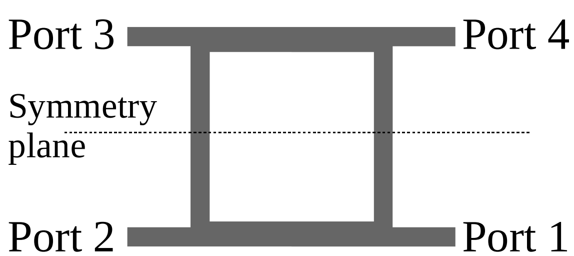

FIGURE 9. Symmetry plane of a quadrature hybrid.

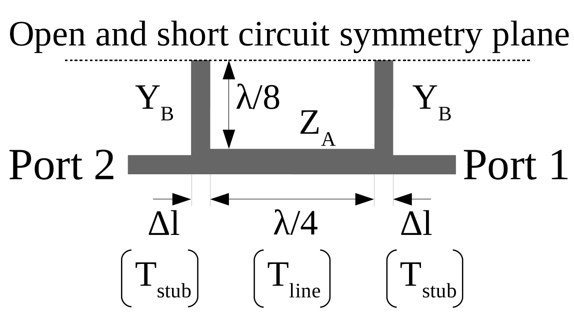

FIGURE 10. Even and odd mode 2-port network for a quadrature hybrid.

A symmetrical four-port network can be analyzed in terms of even and odd modes with respect to the plane of symmetry [33]. The transmission parameter matrix $\mathbf{T}$, or ABCD-matrix, is used to obtain the transmission and reflection characteristics of the hybrids. The circuits are split up into three parts, representing the stubs and the series quarter wavelength transmission line. The propagation coefficient of a transmission line is $\gamma = \alpha + j\beta$. The parameter α is the attenuation constant and β is the phase constant. For a lossless transmission line $\alpha = 0$. The phase constant for the ideal case analysis was set to $\beta\ell = (2\pi/\lambda)(\lambda/4) = \pi/2$ where ℓ is the length of the line. In order to analyze the effect of frequency deviation, the phase constants are changed to $\beta\ell = (2\pi/\lambda)(\lambda_0/4)$, where λ is the wavelength of the frequency of interest and λ_0 is the wavelength of the design frequency.

The odd mode analysis for a quadrature hybrid with short circuited $\lambda/8$ stubs is

$$Z_A = \frac{Z_0}{\sqrt{2}}, \tag{14}$$

$$\mathbf{T_1^o} = \begin{bmatrix} 1 & 0 \\ \dfrac{Z_0}{jZ_0 \tan(\pi\lambda_0/4\lambda)} & 1 \end{bmatrix}, \tag{15}$$

$$\mathbf{T_2^o} = \begin{bmatrix} \cos(\pi\lambda_0/2\lambda) & jZ_A \sin(\pi\lambda_0/2\lambda) \\ j\sin(\pi\lambda_0/2\lambda)/Z_A & \cos(\pi\lambda_0/2\lambda) \end{bmatrix}, \tag{16}$$

$$\mathbf{T_3^o} = \begin{bmatrix} 1 & 0 \\ \dfrac{Z_0}{jZ_0 \tan(\pi\lambda_0/4\lambda)} & 1 \end{bmatrix}, \tag{17}$$

$$\mathbf{T^o} = \mathbf{T_1^o} \cdot \mathbf{T_2^o} \cdot \mathbf{T_3^o} \tag{18}$$

$$= \begin{bmatrix} A_{\text{odd}} & B_{\text{odd}} \\ C_{\text{odd}} & D_{\text{odd}} \end{bmatrix}. \tag{19}$$

The parameters $\mathbf{T_1^o}$ and $\mathbf{T_3^o}$ are the transmission parameter matrices for parallel admittance, where the admittance term is the short circuited $\lambda/8$ stub. $\mathbf{T_2^o}$ is the transmission parameter matrix for a $\lambda/4$ transmission line segment.

The even mode analysis for a quadrature hybrid with open ended $\lambda/8$ stubs is

$$\mathbf{T_1^e} = \begin{bmatrix} 1 & 0 \\ \dfrac{Z_0}{-jZ_0 \cot(\pi\lambda_0/4\lambda)} & 1 \end{bmatrix}, \tag{20}$$

$$\mathbf{T_2^e} = \begin{bmatrix} \cos(\pi\lambda_0/2\lambda) & jZ_A \sin(\pi\lambda_0/2\lambda) \\ j\sin(\pi\lambda_0/2\lambda)/Z_A & \cos(\pi\lambda_0/2\lambda) \end{bmatrix}, \tag{21}$$

$$\mathbf{T_3^e} = \begin{bmatrix} 1 & 0 \\ \dfrac{Z_0}{-jZ_0 \cot(\pi\lambda_0/4\lambda)} & 1 \end{bmatrix}, \tag{22}$$

$$\mathbf{T^e} = \mathbf{T_1^e} \cdot \mathbf{T_2^e} \cdot \mathbf{T_3^e} \tag{23}$$

$$= \begin{bmatrix} A_{\text{even}} & B_{\text{even}} \\ C_{\text{even}} & D_{\text{even}} \end{bmatrix}. \tag{24}$$

The parameters $\mathbf{T_1^e}$ and $\mathbf{T_3^e}$ are the transmission parameter matrices for parallel admittance, where the admittance term is the open ended $\lambda/8$ stub. $\mathbf{T_2^e}$ is the transmission parameter matrix for a $\lambda/4$ transmission line segment. The scattering parameters for a two-port network are calculated as [37]

$$s_i^e = s_i^o = \frac{(A-D)+(BY_o - CZ_0)}{(A+D)+(BY_0+CZ_0)}, \tag{25}$$

$$s_f^e = s_f^o = \frac{2}{(A+D)+(BY_0+CZ_0)}, \tag{26}$$

where $s_i^{e,o}$ and $s_f^{e,o}$ are the reflection and transmission coefficients for even and odd modes, respectively. Considering the quadrature hybrid network with an incident wave at port 1, there will be reflected waves at all four ports. Since the circuit is linear, the incident wave at port 1 can be constructed as the sum of even- and odd-mode components, and their difference giving a zero incident wave at port 4. The four reflected waves are then

$$b_1 = \frac{s_i^e + s_i^o}{2}, \tag{27}$$

$$b_2 = \frac{s_f^e + s_f^o}{2}, \tag{28}$$

$$b_3 = \frac{s_f^e - s_f^o}{2}, \tag{29}$$

$$b_4 = \frac{s_i^e - s_i^o}{2}. \tag{30}$$

The quadrature hybrid has a high degree of symmetry and any port can be used as the input port. The output ports will always be on the opposite side of the input port and the isolated port will be the port remaining. The scattering matrix for a quadrature hybrid is obtained as a transposition of the first row, i.e.,

$$\mathbf{Q} = \begin{bmatrix} b_1 & b_2 & b_3 & b_4 \\ b_2 & b_4 & b_1 & b_3 \\ b_3 & b_1 & b_4 & b_2 \\ b_4 & b_3 & b_2 & b_1 \end{bmatrix}. \tag{31}$$

The even- and odd-mode analysis for a 180°-hybrid is carried out similarly as the analysis for the quadrature hybrid. The stub lengths are now $\lambda/8$ and $3\lambda/8$.

$$Z_{\text{stub}} = \sqrt{2}Z_0, \tag{32}$$

$$Z_{\text{series}} = \sqrt{2}Z_0, \tag{33}$$

$$\mathbf{T_1^o} = \begin{bmatrix} 1 & 0 \\ \dfrac{Z_0}{jZ_{\text{stub}}\tan(\pi\lambda_0/4\lambda)} & 1 \end{bmatrix}, \tag{34}$$

$$\mathbf{T_2^o} = \begin{bmatrix} \cos(\pi\lambda_0/2\lambda) & jZ_{\text{series}}\sin(\pi\lambda_0/2\lambda) \\ j\sin(\pi\lambda_0/2\lambda)/Z_{\text{series}} & \cos(\pi\lambda_0/2\lambda) \end{bmatrix}, \tag{35}$$

$$\mathbf{T_3^o} = \begin{bmatrix} 1 & 0 \\ \dfrac{Z_0}{jZ_{\text{stub}}\tan(3\pi\lambda_0/4\lambda)} & 1 \end{bmatrix}, \tag{36}$$

$$\mathbf{T^o} = \mathbf{T_1^o}\cdot\mathbf{T_2^o}\cdot\mathbf{T_3^o} \tag{37}$$

$$= \begin{bmatrix} A_{\text{odd}} & B_{\text{odd}} \\ C_{\text{odd}} & D_{\text{odd}} \end{bmatrix}, \tag{38}$$

The parameters $\mathbf{T_1^o}$ and $\mathbf{T_3^o}$ are the transmission parameter matrices for parallel admittance, where the admittance terms are the short circuited $\lambda/8$ and $3\lambda/8$ stubs. $\mathbf{T_2^o}$ is the transmission parameter matrix for a $\lambda/4$ transmission line segment.

$$\mathbf{T_1^e} = \begin{bmatrix} 1 & 0 \\ \dfrac{Z_0}{-jZ_{\text{stub}}\cot(\pi\lambda_0/4\lambda)} & 1 \end{bmatrix}, \tag{39}$$

$$\mathbf{T_2^e} = \begin{bmatrix} \cos(\pi\lambda_0/2\lambda) & jZ_{\text{series}}\sin(\pi\lambda_0/2\lambda) \\ j\sin(\pi\lambda_0/2\lambda)/Z_{\text{series}} & \cos(\pi\lambda_0/2\lambda) \end{bmatrix}, \tag{40}$$

$$\mathbf{T_3^e} = \begin{bmatrix} 1 & 0 \\ \dfrac{Z_0}{-jZ_{\text{stub}}\cot(3\pi\lambda_0/4\lambda)} & 1 \end{bmatrix}, \tag{41}$$

$$\mathbf{T^e} = \mathbf{T_1^e}\cdot\mathbf{T_2^e}\cdot\mathbf{T_3^e} \tag{42}$$

$$= \begin{bmatrix} A_{\text{even}} & B_{\text{even}} \\ C_{\text{even}} & D_{\text{even}} \end{bmatrix}. \tag{43}$$

$\mathbf{T_1^e}$ and $\mathbf{T_3^e}$ are the transmission parameter matrices for parallel admittance, where the admittance terms are the open ended $\lambda/8$ and $3\lambda/8$ stubs. $\mathbf{T_2^e}$ is the transmission parameter matrix for a $\lambda/4$ transmission line segment. The scattering parameters for a two-port network are calculated as

$$s_i^e = \frac{2\,A_{\text{even}} + (BY_0 - CZ_0)}{BY_0 + CZ_0}, \tag{44}$$

$$s_i^o = \frac{-2\,A_{\text{even}} + (BY_0 - CZ_0)}{BY_0 + CZ_0}, \tag{45}$$

$$s_f^e = s_f^o = \frac{2}{BY_0 + CZ_0}, \tag{46}$$

where $s_i^{e,o}$ and $s_f^{e,o}$ are the reflection and transmission coefficients for even and odd modes, respectively. The four reflected waves become

$$b_1 = \frac{s_i^e - s_i^o}{2}, \tag{47}$$

$$b_2 = \frac{s_f^e + s_f^o}{2}, \tag{48}$$

$$b_3 = \frac{s_i^e + s_i^o}{2}, \tag{49}$$

$$b_4 = \frac{s_f^e - s_f^o}{2}, \tag{50}$$

and the scattering matrix for a 180°-hybrid reads

$$\mathbf{S} = \begin{bmatrix} b_1 & b_2 & b_3 & b_4 \\ b_2 & b_4 & b_1 & -b_3 \\ b_3 & b_1 & b_4 & b_2 \\ b_4 & -b_3 & b_2 & b_1 \end{bmatrix}. \tag{51}$$

In an ideal situation, the signal of the ambient transmitter is perfectly removed at the receiver end. The isolation between the backscattered signal and the ambient signal is infinite. However, the isolation starts to degrade when the frequency of the backscattered signal deviates from the design frequency or the bandwidth of the bacscattered signal is increased. By using these new scattering matrices **Q** and **S**, Equations (31) and (51) correspondingly, in (13) instead of the ideal ones, the effect of frequency deviation or increase in bandwidth is seen as the isolation comes down. Fig. 11 shows how the isolation is degrading as the bandwidth of the

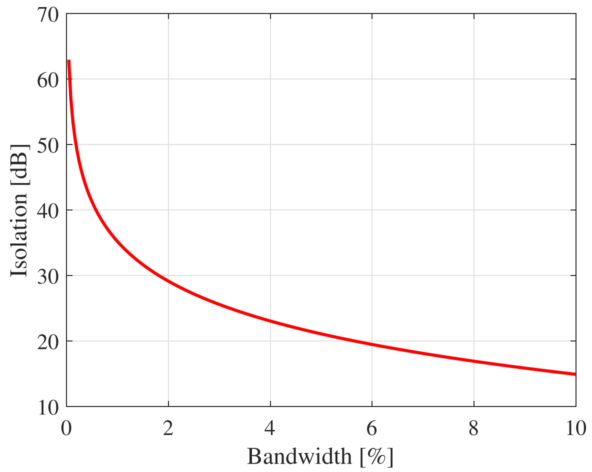

FIGURE 11. Isolation of the antenna system vs. bandwidth percentage.

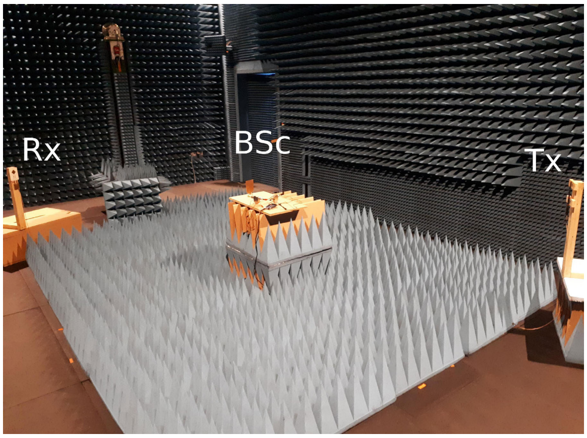

FIGURE 12. Measurement setup in the an-echoic RF-chamber.

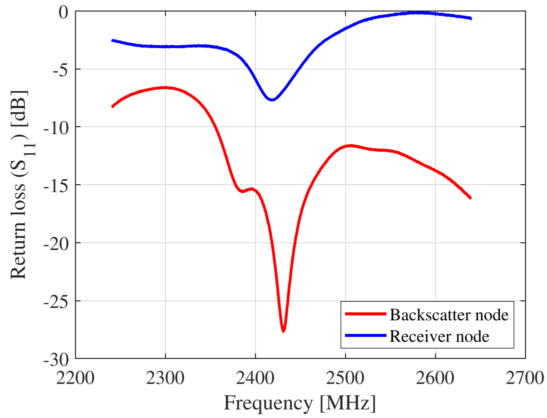

FIGURE 13. Measured return losses for backscatter device and receiver side antennas.

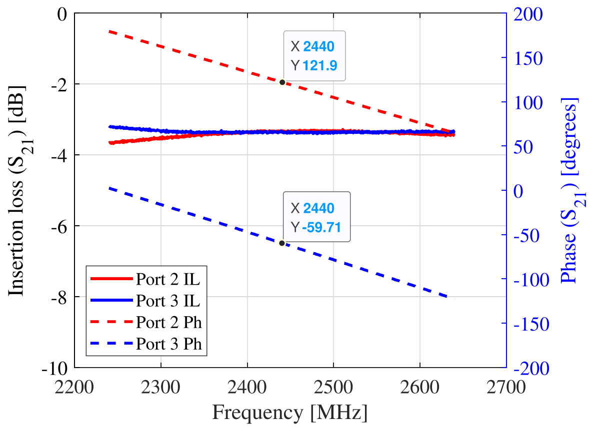

FIGURE 14. Measured insertion loss and phase response for the 180°-hybrid.

signal compared to the design frequency is increased. The bandwidth is expressed as a percentage value of the design frequency. The proposed system offers more than 35 dB isolation between the backscattered and ambient signals, if the bandwidth is less than one percent.

V. PERFORMANCE EVALUATION

The measured reflection losses for the prototype antennas are presented in Fig. 13. The circularly polarized antenna used in the backscatter node has return loss better than −20 dB at the 2.44 GHz frequency. The antenna and the 180°-hybrid combination used at the receiver exhibits poorer performance. The return loss at the same frequency is only around −6 dB. The insertion loss and corresponding phase response of 180°-hybrid was measured separately. The results are presented in Fig. 14. The insertion loss is even across the frequency range of interest and the phase difference between ports 2 and 3 is almost constant 180°, as it should be. The phase difference at the 2.44 GHz frequency is 180.6°.

The performance of the proposed system was evaluated using the antenna prototype shown in Fig. 5. The measurements were carried out in an an-echoic RF-chamber, the distance between the ambient transmitter and the receiver was five meters. The backscatter device was set on the line between the transmitter and receiver. The ambient transmitter is on the right side of Fig. 12, the receiver antenna is on the left side, and the backscatter device is in the middle of the picture. The measurement setup was chosen to be the worst-case scenario, as the ambient transmitter is now directly in front of the receiver antenna, where the receiver antenna gain is at its highest.

The ambient signal used in these measurements was an unmodulated 2.44 GHz carrier wave generated with Rohde&Schwarz SMBV100A Vector Signal Generator. The backscattered signal was a 50 kHz OOK square wave. The evaluation board of the backscatter device was controlled with Arduino Mega 2560 and the signal was received with NI USRP-2932 software-defined radio. The measurements were conducted with two different antenna setups. In both the measurements, the ambient transmitter antenna and the receiver antenna of the backscatter device were linearly polarized whip antennas. In the first measurement, the transmitting antenna of the backscatter device and the antenna at

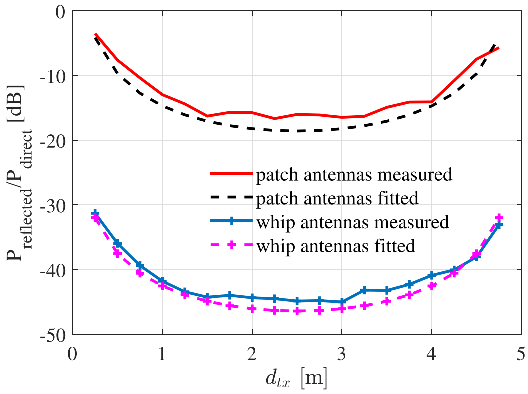

FIGURE 15. Compensated ratio of reflected and direct path power.

the receiver end were circularly polarized patch antennas, including the 180°-hybrid at the receiver. In the second measurement also these two antennas were linearly polarized whip antennas. Both antenna setups were measured, and the ratio between the direct path power and reflected power at the receiver were recorded. The reflected part of the signal observed at the receiver was separated from the direct path signal with a comb filter.

The reflected power values at the receiver were not the same for both antenna types. The difference in observed reflected power can be explained by difference in antenna gains, and slight antenna misalignment. The antenna gains for circularly polarized antennas include the losses caused by the hybrids. With accurate alignment, the difference due to the antennas was roughly 2.5 dB in favor of the whip antennas. Despite the 180° hybrid causing a 3 dB loss for the circular polarization case, the smaller difference can be explained with increased directivity of the circular polarization antennas. However, when measuring the reflected power, the antennas were rarely aligned that well, making the difference larger. To take this into account, an additional measurement was done in every position. After measuring the backscattered signal, a −20 dBm signal was fed straight to the backscatter switch without moving the antennas, and the power was measured at the receiver. This was done with both the whip antennas and the patch antennas. The difference in each position is assumed to consist of antenna gains and misalignment losses, which are taken into account in the results.

When the misalignment and different antenna gains are compensated, the reflected powers for whip and patch antennas are very close. The direct path signal powers were −44.2 dBm when using the whip antenna at the receiver and −71.8 dBm when using the patch antenna at the receiver. With the misalignment compensated, the ratio of reflected and direct path signals is on average 25.3 dB higher in the circular polarization case. The compensated power ratio measurements are presented in Fig. 15. The fitted lines are minimum mean squared error estimates of form $A/(r_{\text{tx}}^2 \cdot r_{\text{rx}}^2)$, r_{tx} and r_{rx} being the distances from the backscatter device to the transmitter and receiver correspondingly, and A being a fitted constant. This model corresponds to the power-ratio depicted in (4), when all constants are merged in to the parameter A.

VI. CONCLUSION

In this paper, we proposed a method to separate the direct and scattered path components in AmBC system by introducing polarization conversion between them. Our design is targeted for scenarios where the ambient signal source uses linearly polarized antennas. We proposed a simple backscatter device capable of doing on-off-keying that converts the linear polarization to circular polarization. For the receiver, we proposed a dual-polarization system consisting of a circularly polarized antenna and a 180°-hybrid. The receiver estimates the Stokes parameter V, i.e. the difference between right- and left-hand circularly polarized field strengths. Hence, a linearly polarized ambient signal is canceled out, while the circularly polarized backscattered signal is received. Due to the ambient signal cancelling properties of the dual-polarization arrangement, also reflected signal components originating from the ambient transmitter are cancelled out.

In practice, the antenna is never ideal so the linearly polarized direct path component cannot be completely cancelled at the receiver. Factors that affect the performance include the symmetry of the receiver gain for the right- and left-hand circularly polarized fields and bandwidth of the ambient signal. The manufacturing accuracy of the dual-polarization antenna system affects directly the isolation between the ambient and backscattered signals. Even if the left- and right-hand circularly polarized signal paths are symmetrical, but the frequency of operation is not the same as the design frequency, the isolation worsens as seen in Fig. 11. We showed that in an-echoic RF-chamber, our proposed setup could achieve more than 25 dB isolation between the backscattered component and the ambient component for narrow band signals. Despite the imperfections in manufacturing the antenna and hybrid circuit prototypes, our design is based on robust operation principles. The proposed system concept can thus help to reduce the required dynamic range for the AmBC receiver.

REFERENCES

[1] H. Stockman, "Communication by means of reflected power," *Proc. IRE*, vol. 36, no. 10, pp. 1196–1204, Oct. 1948.

[2] V. Liu, A. Parks, V. Talla, S. Gollakota, D. Wetherall, and J. R. Smith, "Ambient backscatter: Wireless communication out of thin air," in *Proc. ACM SIGCOMM*, New York, NY, USA, 2013, pp. 39–50, doi: 10.1145/2486001.2486015.

[3] W. Anran, I. Vikram, T. Vamsi, S. Joshua, and G. Shyamnath, "FM backscatter: Enabling connected cities and smart fabrics," in *Proc. NSDI*, New York, NY, USA, Feb. 2017, pp. 243–258.

[4] C. Yang, J. Gummeson, and A. Sample, "Riding the airways: Ultra-wideband ambient backscatter via commercial broadcast systems," in *Proc. IEEE Conf. Comput. Commun.*, Piscataway, NJ, USA, May 2017, pp. 1–9.

[5] A. N. Parks, A. P. Sample, Y. Zhao, and J. R. Smith, "A wireless sensing platform utilizing ambient RF energy," in *Proc. IEEE Topical Conf. Biomed. Wireless Technol., Netw., Sens. Syst.*, Austin, TX, USA, Jan. 2013, pp. 127–129.

[6] A. N. Parks and J. R. Smith, "Sifting through the airwaves: Efficient and scalable multiband RF harvesting," in *Proc. IEEE Int. Conf. RFID (IEEE RFID)*, Piscataway, NJ, USA, Apr. 2014, pp. 74–81.

[7] J. F. Ensworth and M. S. Reynolds, "Every smart phone is a backscatter reader: Modulated backscatter compatibility with Bluetooth 4.0 low energy (BLE) devices," in *Proc. IEEE Int. Conf. RFID (RFID)*, San Diego, CA, USA, Apr. 2015, pp. 78–85.

[8] V. Iyer, V. Talla, B. Kellogg, S. Gollakota, and J. Smith, "Inter-technology backscatter: Towards Internet connectivity for implanted devices," in *Proc. Conf. ACM SIGCOMM Conf.*, New York, NY, USA, 2016, pp. 356–369.

[9] F. Sangare and Z. Han, *RF Energy Harvesting Networks: Existing Techniques and Hardware Technology*. Cham, Switzerland: Springer, 2018, pp. 189–239, ch. 7.

[10] B. Kellogg, V. Talla, S. Gollakota, and J. R. Smith, "Passive Wi-Fi: Bringing low power to Wi-Fi transmissions," in *Proc. 13th USENIX Conf. Netw. Syst. Design Implement.*, Santa Clara, CA, USA, 2016, pp. 151–164.

[11] P. Zhang, M. Rostami, P. Hu, and D. Ganesan, "Enabling practical backscatter communication for on-body sensors," in *Proc. Conf. ACM SIGCOMM Conf.*, New York, NY, USA, 2016, pp. 370–383.

[12] V. Talla, B. Kellogg, B. Ransford, S. Naderiparizi, J. R. Smith, and S. Gollakota, "Powering the next billion devices with Wi-Fi," *Commun. ACM*, vol. 60, no. 3, pp. 83–91, Feb. 2017.

[13] H. Hwang, J.-H. Lim, J.-H. Yun, and B. Jeong, "Pattern-based decoding for Wi-Fi backscatter communication of passive sensors," *Sensors*, vol. 19, no. 5, p. 1157, Mar. 2019.

[14] R. Duan, X. Wang, H. Yigitler, M. U. Sheikh, R. Jantti, and Z. Han, "Ambient backscatter communications for future Ultra-Low-Power machine type communications: Challenges, solutions, opportunities, and future research trends," *IEEE Commun. Mag.*, vol. 58, no. 2, pp. 42–47, Feb. 2020.

[15] R. Duan, E. Y. Menta, H. Yigitler, R. Jäntti, and Z. Han, "Hybrid beamformer design for high dynamic range ambient backscatter receivers," in *Proc. IEEE ICC Workshops*, Shanghai, China, May 2019, pp. 1–6.

[16] X. Wang, R. Duan, H. Yigitler, E. Menta, and R. Jantti, "Machine learning-assisted detection for BPSK-modulated ambient backscatter communication systems," in *Proc. IEEE Global Commun. Conf. (GLOBECOM)*, Waikoloa, HI, USA, Dec. 2019, pp. 1–6.

[17] N. Van Huynh, D. T. Hoang, X. Lu, D. Niyato, P. Wang, and D. I. Kim, "Ambient backscatter communications: A contemporary survey," *IEEE Commun. Surveys Tuts.*, vol. 20, no. 4, pp. 2889–2922, 3rd Quart., 2018.

[18] M. A. ElMossallamy, Z. Han, M. Pan, R. Jantti, K. G. Seddik, and G. Y. Li, "Backscatter communications over ambient OFDM signals using null subcarriers," in *Proc. IEEE Global Commun. Conf. (GLOBECOM)*, Abu Dhabi, United Arab Emirates, Dec. 2018, pp. 1–6.

[19] M. A. ElMossallamy, M. Pan, R. Jantti, K. G. Seddik, G. Y. Li, and Z. Han, "Noncoherent backscatter communications over ambient OFDM signals," *IEEE Trans. Commun.*, vol. 67, no. 5, pp. 3597–3611, May 2019.

[20] R. Duan, R. Jantti, H. Yigitler, and K. Ruttik, "On the achievable rate of bistatic modulated rescatter systems," *IEEE Trans. Veh. Technol.*, vol. 66, no. 10, pp. 9609–9613, Oct. 2017.

[21] D. Darsena, G. Gelli, and F. Verde, "Modeling and performance analysis of wireless networks with ambient backscatter devices," *IEEE Trans. Commun.*, vol. 65, no. 4, pp. 1797–1814, Apr. 2017.

[22] R. Duan, R. Jantti, M. ElMossallamy, Z. Han, and M. Pan, "Multi-antenna receiver for ambient backscatter communication systems," in *Proc. IEEE 19th Int. Workshop Signal Process. Adv. Wireless Commun. (SPAWC)*, Kalamata, Greece, Jun. 2018, pp. 1–5.

[23] P. Zhang, D. Bharadia, K. Joshi, and S. Katti, "HitchHike: Practical backscatter using commodity WiFi," in *Proc. 14th ACM Conf. Embedded Netw. Sensor Syst.*, New York, NY, USA, Nov. 2016, pp. 259–271.

[24] A. Varshney, O. Harms, C. Pérez-Penichet, C. Rohner, F. Hermans, and T. Voigt, "LoRea: A backscatter architecture that achieves a long communication range," in *Proc. 15th ACM Conf. Embedded Netw. Sensor Syst.*, Nov. 2017, pp. 1–4.

[25] J. Zhao, W. Gong, and J. Liu, "X-tandem: Towards multi-hop backscatter communication with commodity WiFi," in *Proc. 24th Annu. Int. Conf. Mobile Comput. Netw.*, 2018, pp. 497–511, doi: 10.1145/3241539.3241553.

[26] J. Zhao, W. Gong, and J. Liu, "Spatial stream backscatter using commodity WiFi," in *Proc. 16th Annu. Int. Conf. Mobile Syst., Appl., Services*, Jun. 2018, pp. 191–203, doi: 10.1145/3210240.3210329.

[27] A. N. Parks, A. Liu, S. Gollakota, and J. R. Smith, "Turbocharging ambient backscatter communication," in *Proc. ACM Conf. SIGCOMM*, New York, NY, USA, 2014, pp. 619–630.

[28] R. Fara, D.-T. Phan-Huy, A. Ourir, Y. Kokar, J.-C. Prevotet, M. Helard, M. Di Renzo, and J. De Rosny, "Polarization-based reconfigurable tags for robust ambient backscatter communications," *IEEE Open J. Commun. Soc.*, vol. 1, pp. 1140–1152, 2020.

[29] C. Carrender, "Full-spectrum passive communication system and method," U.S. Patent 6 970 089 B2, Jul. 3, 2002.

[30] S. S. Gao, Q. Luo, and F. Zhu, *Circularly Polarized Antennas*. Hoboken, NJ, USA: Wiley, 2013.

[31] J. D. Griffin and G. D. Durgin, "Complete link budgets for backscatter-radio and RFID systems," *IEEE Antennas Propag. Mag.*, vol. 51, no. 2, pp. 11–25, Apr. 2009.

[32] B. W. Pike, "Power transfer between two antennas with special reference to polarization," Air Force Western Test RANGE, Vandenberg, CA, USA, Tech. Rep. AFWTR-TR-65-1, 1965.

[33] D. M. Pozar, *Microwave Engineering*, 4th ed. Hoboken, NJ, USA: Wiley, 2012.

[34] R. Bancroft, *Microstrip Printed Antenna Design*. Raleigh, NC, USA: Institution of Engineering and Technology, 2009.

[35] *HMC270A Datasheet and Product Info*. Accessed: Jun. 2, 2019. [Online]. Available: https://www.analog.com/en/products/hmc270a.html#product-overview

[36] J. Wang, C. Choi, and R. Moore, "Precision experimental characterization of the scattering and radiation properties of antennas," *IEEE Trans. Antennas Propag.*, vol. 30, no. 1, pp. 108–112, Jan. 1982.

[37] E. Fooks and R. Zakarevičius, *Microwave Engineering Using Microstrip Circuits*. Upper Saddle River, NJ, USA: Prentice Hall, 1990.

JARI LIETZÉN received the M.Sc. degree (Hons.) in communications engineering from Aalto University, Finland, in 2016, where he is currently pursuing the Ph.D. degree. His research interests include error correction and key growing protocols in quantum key distribution and backscatter communications.

ALEKSI LILJEMARK received the B.Sc. degree in information technology from Aalto University, in 2019. He is currently pursuing the M.Sc. degree in communications engineering. He has been working as a Research Assistant with the Department of Communications and Networking, School of Electrical Engineering, Aalto University, since 2018. His research interest includes ambient backscatter communication.

RUIFENG DUAN (Member, IEEE) received the M.Sc.(Tech.) and D.Sc.(Tech.) degrees in telecommunications engineering from the University of Vaasa, Finland, in 2008 and 2014, respectively. He is currently with Nokia Mobile Network, Finland, and with the Department of Communications and Networking, Aalto University, Finland. He held a visiting position at the Department of Electrical and Computer Engineering, Prairie View A& M University (a member of Texas A& M University System). His current research interests include 5G New Radio, random matrix theory, extreme value theory, ambient backscatter communication, and ultra-reliable low latency communications. In addition, he received the Vaasa University Foundation Scholarship for the academic years of 2010–2011 and 2011–2012, the Ella and Georg Ehrnrooth Foundation Scholarship in 2010, the IEEE GLOBECOM 2010 Early-Bird Student Award, and the Best Paper Award at The International Symposium on Networks, Computers, and Communications, in June 2018.

RIKU JÄNTTI (Senior Member, IEEE) received the M.Sc. degree (Hons.) in electrical engineering and the D.Sc. degree (Hons.) in automation and systems technology from the Helsinki University of Technology (TKK), in 1997 and 2001, respectively. Prior to joining Aalto (formerly known as TKK) in August 2006, he was a Professor pro tem with the Department of Computer Science, University of Vaasa. He is currently a Full Professor of Communications Engineering and the Head of the Department of Communications and Networking with the School of Electrical Engineering, Aalto University, Finland. His research interests include machine type communications, cloud-based radio access networks, backscatter communications, quantum communications, and RF Inference. He is an Associate Editor of IEEE Transactions on Vehicular Technology. He has been an IEEE VTS Distinguished Lecturer (Class 2016).

VILLE VIIKARI (Senior Member, IEEE) was born in Espoo, Finland, in 1979. He received the M.Sc. (Tech.) and D.Sc. (Tech.) degrees (Hons.) in electrical engineering from the Helsinki University of Technology (TKK), Espoo, Finland, in 2004 and 2007, respectively.

From 2001 to 2007, he was with the Radio Laboratory, TKK, where he studied antenna measurement techniques at submillimeter wavelengths and antenna pattern correction techniques. From 2007 to 2012, he was a Research Scientist and a Senior Scientist with the VTT Technical Research Centre, Espoo. He is currently an Associate Professor and the Deputy Head of the Department with the School of Electrical Engineering, Aalto University, Espoo. His research interests include wireless sensors, RFID, radar applications, MEMS, microwave sensors, antennas for mobile networks, RF-powered devices, and antenna measurement techniques.

Dr. Viikari was a recipient of the Young Researcher Award of the Year 2014, presented by the Finnish Foundation for Technology Promotion, IEEE Sensors Council 2010 Early Career Gold Award, the 2008 Young Scientist Award of the URSI XXXI Finnish Convention on Radio Science, Espoo, Finland, and the Best Student Paper Award of the annual symposium of the Antenna Measurement Techniques Association, Newport, RI, USA, from October 2005 to November 2005. He has served as the Chair for the Technical Program Committee of the ESA Workshop on Millimetre-Wave Technology and Applications and the Global Symposium on Millimeter Waves (GSMM) twice, in 2011 and 2016, Espoo, Finland.